Journal of Thermal Science and Technology

Vol.3, No.1, 2008

Numerical Study of Heat Transfer Mechanism in Turbulent Supercritical CO_2 Channel Flow*

Xinliang LI**,***, Katsumi HASHIMOTO†, Yasuhiro TOMINAGA**, Mamoru TANAHASHI** and Toshio MIYAUCHI**

** Department of Mechanical and Aerospace Engineering, Tokyo Institute of Technology
2-12-1 Ookayama, Meguro-ku, Tokyo 152-8550, Japan
E-mail: mtanahas@mes.titech.ac.jp

*** LNM, Institute of Mechanics, Chinese Academy of Sciences
No. 15, Beisihuanxi-Road, Beijing, 100080, China

† Central Research Institute of Electric Power Industry
2-6-1, Nagasaka,Yokosuka-shi, Kanagawa 240-0196, Japan

Abstract

Direct numerical simulation (DNS) of supercritical CO_2 turbulent channel flow has been performed to investigate the heat transfer mechanism of supercritical fluid. In the present DNS, full compressible Navier-Stokes equations and Peng-Robison state equation are solved. Due to effects of the mean density variation in the wall normal direction, mean velocity in the cooling region becomes high compared with that in the heating region. The mean width between high- and low-speed streaks near the wall decreases in the cooling region, which means that turbulence in the cooling region is enhanced and lots of fine scale eddies are created due to the local high Reynolds number effects. From the turbulent kinetic energy budget, it is found that compressibility effects related with pressure fluctuation and dilatation of velocity fluctuation can be ignored even for supercritical condition. However, the effect of density fluctuation on turbulent kinetic energy cannot be ignored. In the cooling region, low kinematic viscosity and high thermal conductivity in the low speed streaks modify fine scale structure and turbulent transport of temperature, which results in high Nusselt number in the cooling condition of the supercritical CO_2.

Key words : Turbulent Heat Transfer, Supercritical Flow, Direct Numerical Simulation, Turbulent Channel Flow

1. INTRODUCTION

The supercritical fluid has both gas-like and liquid-like properties, and it is frequently used in many industrial applications such as chemical process and food production. Since the supercritical fluid shows very strong heat transport capability near its pseudo-critical point, it is considered to be a good working fluid in heat transfer. For example, in supercritical water-cooled reactor, the supercritical water is used as the medium of heat transfer instead of liquid water. The supercritical water-cooled reactor has higher heat transfer efficiency, less complexity and more compact than the normal light water reactor[1]. Similar to supercritical water, supercritical CO_2 is also one kind of promising heat transfer medium. Since the critical temperature of CO_2 (about 304K or 31°C) is near normal temperature, it is a good refrigerant in hot water heating. Moreover, a CO_2 heat pump for domestic hot tap water supplier with high heat transfer efficiency has been developed and commercialized in Japan. As addressed in Hashimoto et al.[2], to develop higher performance and further compact heat pump, high-pressure side heat exchanger of the CO_2 heat pump should have better performance and be smaller than conventional one. Therefore, it is very important to understand the heat transfer

*Received 12 Nov., 2007 (No. 07-0702)
[DOI: 10.1299/jtst.3.112]

mechanism of supercritical flow. In many cases, the supercritical flows are in turbulent or transitional state and the fluid flow is rather complicated. However, the research works on turbulent (or transitional) supercritical flow are very rare until now, and the research on turbulent supercritical flow is very useful to improve the industrial applications of supercritical fluid. Direct numerical simulation (DNS) plays an important role in study of turbulent flow as a strong research tool. However, the DNS study of supercritical turbulent flow is very few because of its complexity. Hashimoto et al.[2] have conducted DNS of supercritical CO_2 turbulent channel flow, and investigated the near-wall heat transfer mechanism. In their DNS, effects of drastic change of Prandtl number and viscosity near the pseudo-critical point are considered under the incompressible assumption where the effects of density variation are neglected. DNS of turbulent CO_2 fluid at supercritical pressure in heated vertical tubes has been performed by Bae et al.[3] with low Mach number approximation. In their work, temperature range includes the pseudo-critical region and buoyancy effects on turbulent statistics were investigated. It should be noted that low Mach number approximation can not represent acoustic interactions and compressibility effect exactly.

In this research, DNS of supercritical CO_2 turbulent channel flow is performed to investigate the turbulent heat transfer mechanism of supercritical flow. Full compressible Navier-Stokes equations are solved with temperature dependence of physical properties of CO_2. DNS of full compressible Navier-Stokes equation takes an advantage that all compressibility effects can be considered. However, DNS is suffered by the severe time step restriction as addressed in Bae et al.[3]. Since the background of this study is development of the supercritical CO_2 domestic heat pump with high efficiency, the temperature range in this DNS is chosen within normal temperature, and forced convective heat transfer is focused by neglecting buoyancy effects.

2. NUMERICAL METHOD

Full compressible Navier-Stokes equations and energy conservation equation are solved to take into account temperature dependence of thermal and transport properties of the supercritical fluid. Followings are continuity, Navier-Stokes and energy conservation equations analyzed in this study.

$$\frac{\partial \rho}{\partial t} + \frac{\partial (\rho u_i)}{\partial x_i} = 0, \tag{1}$$

$$\rho \frac{\partial u_i}{\partial t} + \rho u_j \frac{\partial u_i}{\partial x_j} = -\frac{\partial p}{\partial x_i} + \frac{\partial \tau_{ij}}{\partial x_j} + f_i, \tag{2}$$

$$\rho \left(\frac{\partial h}{\partial t} + u_j \frac{\partial h}{\partial x_j} \right) = \frac{\partial}{\partial x_j} \left(k \frac{\partial T}{\partial x_j} \right) + \frac{\partial u_i}{\partial x_j} \tau_{ji} + \frac{\partial p}{\partial t} + u_j \frac{\partial p}{\partial x_j} + f_i u_i, \tag{3}$$

where τ_{ij} is the shear stress tensor defined as

$$\tau_{ij} = \mu \left(\frac{\partial u_i}{\partial x_j} + \frac{\partial u_j}{\partial x_i} - \frac{2}{3} \frac{\partial u_k}{\partial x_k} \delta_{ij} \right), \tag{4}$$

and $h = e + p/\rho$ is the enthalpy. $f_i = f\delta_{i1}$ is a uniform body force to drive the channel flow. Since, the pressure fluctuation is very low because of low Mach number, the enthalpy can be assumed only the function of temperature, i.e. $h = h(P_0, T)$, where P_0 is 8MPa in this study. The term $\partial p/\partial t$ in Eq. 3 can be ignored by the same reason. Considering $c_p = (\partial h/\partial T)_p$, the energy equation (Eq. 3) can be rewrited as following:

$$\rho c_p \left(\frac{\partial T}{\partial t} + u_j \frac{\partial T}{\partial x_j} \right) = \frac{\partial}{\partial x_j} \left(k \frac{\partial T}{\partial x_j} \right) + \frac{\partial u_i}{\partial x_j} \tau_{ji} + u_j \frac{\partial p}{\partial x_j} + f_i u_i. \tag{5}$$

Table 1 NUMERICAL PARAMETERS

ID	Re_m	Ma_m	T_w	T_0	$L_x \times L_y \times L_z$	$N_x \times N_y \times N_z$
Case 1	2800	0.2	311.15K ~ 321.15K	316.15K	$48\pi\delta \times 2\delta \times 2\pi\delta$	$2304 \times 193 \times 160$
Case 2	2800	0.2	309.15K ~ 319.15K	314.15K	$48\pi\delta \times 2\delta \times 2\pi\delta$	$2880 \times 256 \times 192$

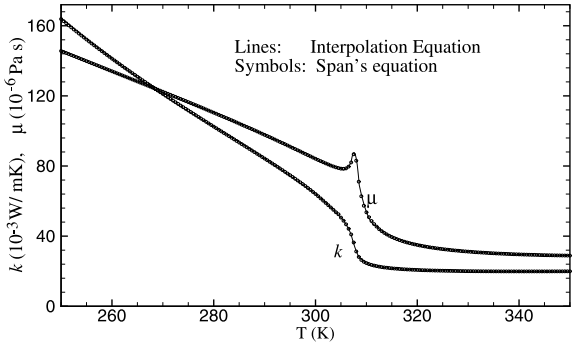

Fig. 1 Thermal conductivity and viscosity for CO_2 at P = 8MPa.

The above conservation equations should be solved with the state equation which gives pressure-density-temperature relationship. The following Peng-Robinson equation[4] is used to estimate pressure from density and temperature.

$$p = \frac{RT}{V_m - b} - \frac{a\alpha}{V_m^2 + 2bV_m^2 - b^2}, \tag{6}$$

where V_m represents the molar volume and $V_m = (0.044\ \text{kg/mol})/\rho$ for CO_2. $R = 8.314472$ J/(mol · K) is the universal gas constant. Other parameters are given as follows:

$$\alpha = [1 + (0.37464 + 1.54226\omega - 0.26992\omega^2)(1 - T_r^{0.5})]^2,$$
$$T_r = T/T_c,$$
$$a = 0.45724R^2T_c^2/p_c,$$
$$b = 0.07780RT_c/p_c,$$

where $T_c = 304.1282$K is the critical temperature and $p_c = 7.3773$MPa is the critical pressure. The acentric factor ω in the Peng-Robinson equation is tuned according to experimental data[5], and set to be $\omega = 0.3$ in this DNS. Since the pressure fluctuation is very small relative to mean pressure (8MPa), the transport and thermal properties such as viscosity (μ), specific heat (c_p) and thermal conductivity (k) are assumed to be only the function of temperature, i.e. $\mu = \mu(P_0, T)$, $c_p = c_p(P_0, T)$, and $k = k(P_0, T)$, where $P_0 = 8$MPa in this study. Partition parabolic interpolation equations are introduced to calculate these properties. In Fig. 1, thermal conductivity and viscosity predicted by the interpolation are compared with those by Span et al.[5]. The interpolated values agree well with the results of Span et al.[5] including near the pseudo-critical point.

To approximate the convective terms in momentum and energy equations, 7th-order upwind finite difference scheme is used. For other terms, 8th-order central finite difference scheme is used. Time advancement is implemented by a 3rd-order TVD type Runge-Kutta scheme[6].

3. DIRECT NUMERICAL SIMULATION

The channel is assumed to be full with supercritical CO_2 at 8MPa. The periodic conditions are adopted in streamwise and spanwise directions by applying periodic wall-temperature in the streamwise direction. Two cases are computed in this research. The difference between the two cases is the wall temperature. The distribution of wall temperatures T_w are shown in Fig. 2. T_w is set to be the maximum value in $4\pi < x < 20\pi$ and the minimum value in $28\pi < x < 44\pi$. The maximum wall temperature is 321.15K for case1 and 319.15K for case2,

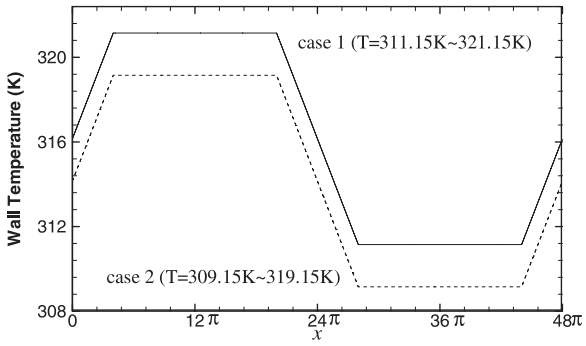

Fig. 2 Distribution of wall temperature.

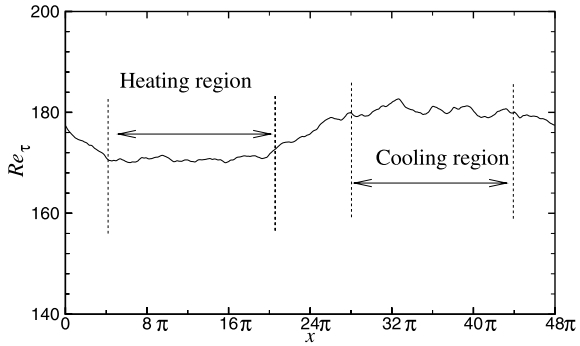

Fig. 3 Distribution of friction Reynolds number in streamwise directions for case1.

and the minimum wall temperature is 311.15K for case1 and 309.15K for case2. DNS is conducted for the temperature range higher than the pseudo-critical temperature for the both cases. Uniform body force is applied to drive the flow. The magnitude of the body force is set to be that for $Re_\tau = 180$ ($Re_m = 2800$) in incompressible channel flow. The numerical parameters are shown in Table 1. Here, Re_m is Reynolds number defined by the mean bulk velocity u_m, the mean density ρ_m, the channel half width δ and the viscosity μ at mean temperature T_0. Ma_m is the Mach number defined by u_m and the sound speed at T_0. T_0 denotes mean temperature of the maximum and minimum wall temperature. In the streamwise direction, length of the computational domain is chosen enough to investigate effects of variable density and physical properties on the turbulence structure and heat transfer. DNS was conducted until statistically steady state.

4. TURBULENCE STATISTICS

In the present DNS, friction Reynolds number(Re_τ) is not constant in the streamwise direction. Figure 3 shows streamwise variation of Re_τ for case1. Since the added body force corresponds to $Re_\tau = 180$ for the incompressible case, Re_τ in Fig. 3 fluctuates near 180. From the characteristics of CO_2 near the pseudo-critical point as shown in Fig. 1, kinematic viscosity ($\nu = \mu/\rho$) is low in the cooling region ($28\pi < x < 44\pi$). Therefore, Re_τ in the cooling region is higher than that in the heating region.

Figure 4 shows mean streamwise velocity profile and Van Direst mean velocity profile at $x = 15.9\pi$ (in the heating region) and $x = 41.4\pi$ (in the cooling region) for case1. The Van Direst mean velocity is defined as

$$U_{VD}^{+} = \int_0^{u^+} \sqrt{\bar{\rho}/\bar{\rho}_w}\, du^+. \tag{7}$$

The mean velocity in the cooling region is much higher than that in the heating region, whereas the Van Direst velocities in two regions agree with each other. These facts suggest that the

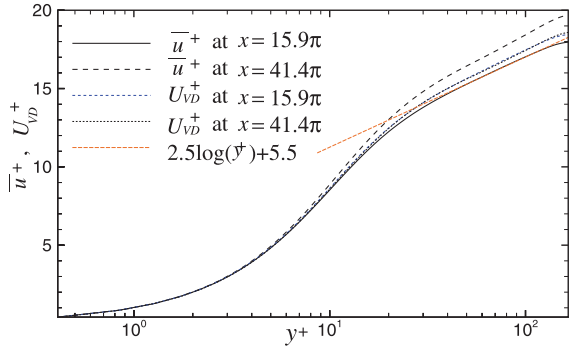

Fig. 4 Profiles of mean velocity and Van Dirst mean velocity for case1.

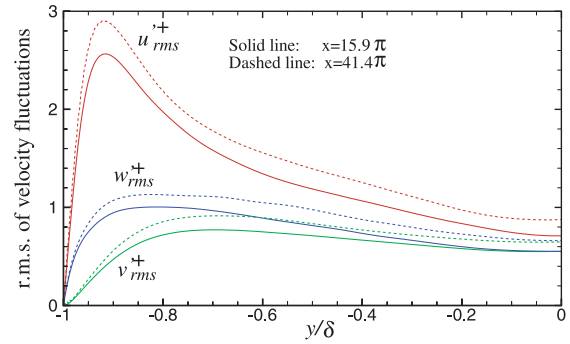

Fig. 5 Profiles of r. m. s. of velocity fluctuations for case1.

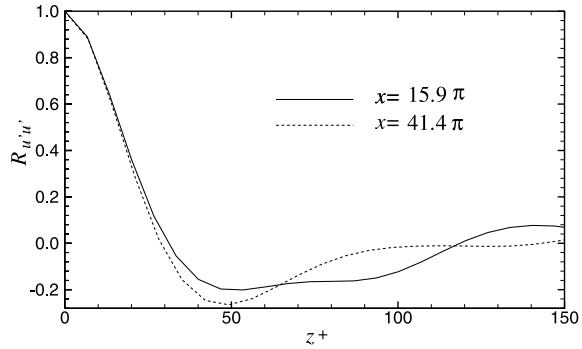

Fig. 6 Autocorrelation function of u' in spanwise direction at $y^+ \approx 5$ for case1.

mean velocities are affected by the density variation, but not by acoustic effects or intrinsic compressibility effects. Figure 5 shows the r. m. s. of velocity fluctuations normalized by local u_τ at $x = 15.9\pi$ and $x = 41.4\pi$ for case1. The r. m. s. of velocity fluctuations in the cooling region is higher than that in the heating region. Therefore, turbulent motion is enhanced in the cooling region and is depressed in the heating region. As turbulent intensities are normalized by local u_τ, the difference between heating and cooling region can not be explained only from physical properties of supercritical CO_2. To interpret this phenomena, turbulent structures should be discussed.

As one of the important near-wall structures, high- and low-speed streaks are well-known. The mean width of the streaks can be estimated from autocorrelation of the streamwise velocity fluctuation. Figure 6 shows two-points autocorrelation function of streamwise velocity fluctuation at $y^+ \approx 5$ for case1. From the location of the minimum value, the mean space between the high- and low-speed streak is estimated to $l^+ = 53.5(l = 0.31\delta)$ in the heating region and $l^+ = 49.2(l = 0.27\delta)$ in the cooling region. This decreasing shows that there are more streaks in the cooling region. It has been shown that near-wall streamwise eddies, which

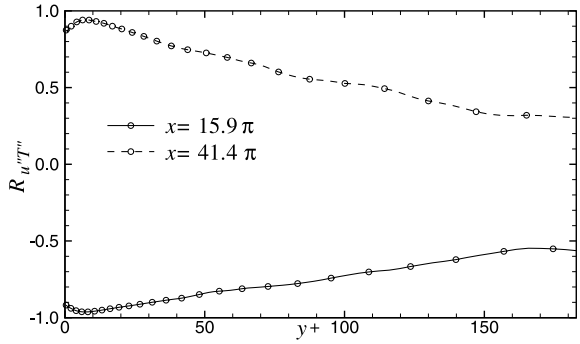

Fig. 7 Distribution of $u'' - T''$ correlations for case1.

is one of coherent fine scale eddies[7], tend to exist near boundary of high- and low-speed streaks. Therefore, the increase of streaks suggests that lots of the coherent fine scale eddies appear. Since the near-wall coherent fine scale eddy has an important role in turbulent heat transfer, the increasing of the coherent fine scale eddy enhances the heat transfer ability of the supercritical flow.

Figure 7 shows correlation coefficients between streamwise velocity fluctuation and temperature fluctuation for case1. The correlations are evaluated from fluctuations based on a density-weighted average (Favre average defined in the next section). There are strong negative correlations in the heating regions and strong positive correlations in the cooling regions, especially, in the near wall regions. This result means that high-speed streaks have low local temperatures in the heating region, and high-speed streaks have high local temperatures in the cooling region. This correlation of turbulent supercritical flow is different from that of ordinary compressible turbulence. In the ordinary compressible wall turbulence under the adiabatic wall condition, the $u'' - T''$ correlation is always negative according to strong Reynolds analogy (SRA) theory[8]. In the cases of unilateral cooling and heating, low speed streaks tends to be near the wall temperature.

5. TURBULENT KINETIC ENERGY BUDGET

The transport equation for turbulent kinetic energy in compressible flows is written as follow:

$$\frac{\partial(\bar{\rho}K)}{\partial t} + C = P + T + \Pi_t + \Pi_d + D + M - \varepsilon, \tag{8}$$

where K and C denote the turbulent kinetic energy and convection terms defined by

$$K = \frac{1}{2}\frac{\overline{\rho u_i'' u_i''}}{\bar{\rho}},$$
$$C = \frac{\partial(\tilde{u}_j \bar{\rho} K)}{\partial x_j}.$$

As for other terms in Eq. 8, P, T, Π_t, Π_d, D, M and ε are the production term, the turbulent diffusion term, the pressure diffusion term, the pressure-dilatation term, the viscous diffusion term, the term associated with density fluctuations and the viscous dissipation term, respectively. Each term is defined as follow:

$$P = -\overline{\rho u_i'' u_j''}\frac{\partial \tilde{u}_i}{\partial x_j},$$
$$T = -\frac{1}{2}\frac{\partial}{\partial x_j}(\overline{\rho u_i'' u_i'' u_j''}),$$
$$\Pi_t = -\frac{\partial}{\partial x_j}(\overline{p' u_j''}),$$

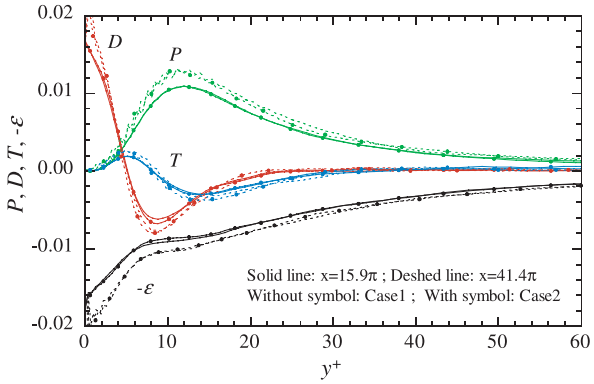

Fig. 8 Distribution of turbulent kinetic energy production term (P), viscous dissipation term (ε), viscous diffusion term (D) and turbulent transport term (T).

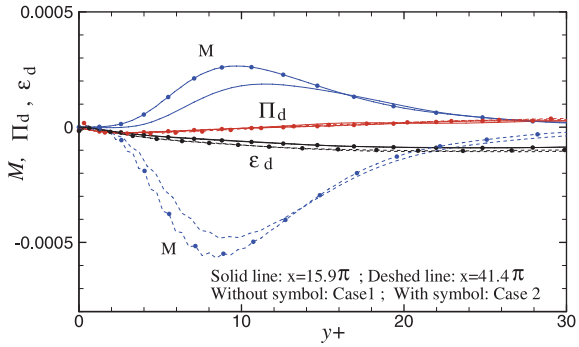

Fig. 9 Distribution of pressure dilatation term (Π_d), dilatation dissipation term (ϵ_d) and the term associated with density fluctuation (M).

$$\Pi_d = \overline{p' \frac{\partial u_i''}{\partial x_i}},$$

$$M = -\bar{u}_i'' \left(\frac{\partial \bar{\tau}_{ij}}{\partial x_j} - \frac{\partial \bar{p}}{\partial x_i} \right),$$

$$D = \frac{\partial}{\partial x_i} \overline{u_i'' \tau_{ij}'},$$

$$\varepsilon = \overline{\tau_{ij}' \frac{\partial u_i''}{\partial x_j}}.$$

In the above expressions, $\tilde{\phi}$ represents the Favre average of ϕ ($= \overline{\rho\phi}/\bar{\rho}$), and $\phi' = \phi - \bar{\phi}$, $\phi'' = \phi - \tilde{\phi}$ are the fluctuations based on Reynolds average and Favre average, respectively.

Turbulent kinetic energy budget at $x = 15.9\pi$ (heating region) and 41.4π (cooling region) are evaluated in this study. The production term, viscous dissipation term, viscous diffusion term and turbulent diffusion term are dominant in the energy equation, and other terms are small relative to these four terms. In Fig. 8, the dominant four terms are compared in the cooling and heating regions for the two cases. This balance of the energy budget is similar to those of incompressible turbulence[7), (9), (10)]. It should be noted that the convection terms are not exactly zero for the present case because of the periodic cooling and heating in the streamwise direction. However, the results of DNS show that the convection terms are very small compared with the major terms. The production term and viscous dissipation terms show large magnitude in the cooling region. In the buffer layer ($y^+ \approx 10 \sim 30$), the increase of the production term balances with that of the viscous dissipation term, which implies that turbulence structure in the buffer layer is significantly different in the cooling and heating region. Near the wall, the viscous diffusion term in the cooling region is larger than that in

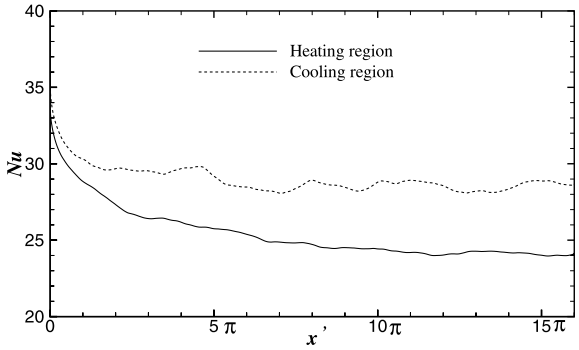

Fig. 10 Distribution of Nusselt number for case1. ($x' = x - 4\pi$ in the heating region, $x' = x - 28\pi$ in the cooling region)

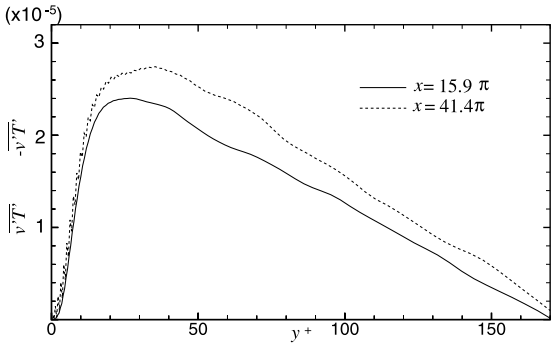

Fig. 11 Distribution of turbulent heat flux for case1.

the heating region due to viscosity variation. Note that oscillations in Fig. 8 is caused by short average time due to the huge DNS, and will disappear if the average was taken in longer time.

In variable density turbulent flows, the pressure-dilatation term, dilatation dissipation term, which is included in the viscous dissipation term (ε), and the term associated with density fluctuation have possibilities to change the energy budget. The dilatation dissipation term is defined as follow:

$$\varepsilon_d = \frac{4}{3}\bar{\mu}\overline{\left(\frac{\partial u_i''}{\partial x_i}\right)^2}. \tag{9}$$

In Fig. 9, these three terms are shown in the cooling and heating region for the two cases. Both of pressure dilatation and dilatation dissipation terms have weak contribution for energy transport, whereas the terms associated with density fluctuation show effective values. These terms show a peak at $y^+ \approx 10$, and the peak value is greater than 5% of the production term. It is well known that compressibility effects always depress the development of turbulence. However, density fluctuations effects do not always work for depression in the present study. These terms show positive values in the heating region and negative values in the cooling region, which means that the density fluctuation effects enhance turbulence in the heating region and depress turbulence in the cooling region. The density fluctuation effects partially offset turbulent kinetic energy in the cooling region. In the cooling region, since the wall temperature is close to the pseudo-critical point, the density fluctuation effect is relatively strong. Therefore, this effect will be more significant if the temperature range was more close to the pseudo-critical point. This is the reason why the term associated with density fluctuation is significant in the cooling region of case 2.

6. HEAT TRANSFER CHARACTERSTIC

Nusselt number is very important property to characterize heat transfer efficiency. Figure 10 shows streamwise variation of Nusselt number in the heating and cooling regions for case1.

Fig. 12 Distribution of kinematic viscosity (a) and thermal conductivity (b) at $y^+ \approx 5$ for case1.

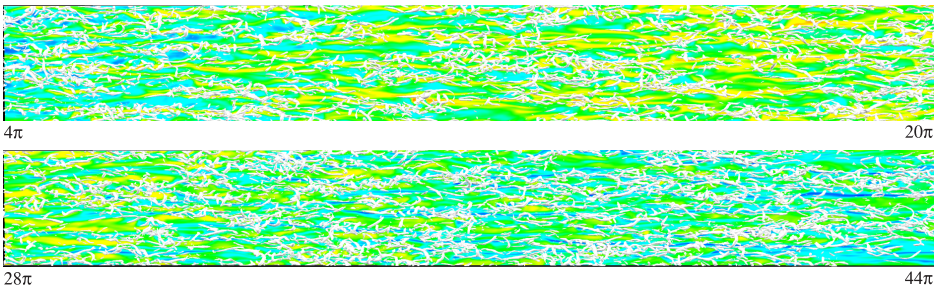

Fig. 13 Contour of temparature on a $x-z$ plane ($y^+ \approx 10$) with iso-surface of $Q = 1.0$ for case1.

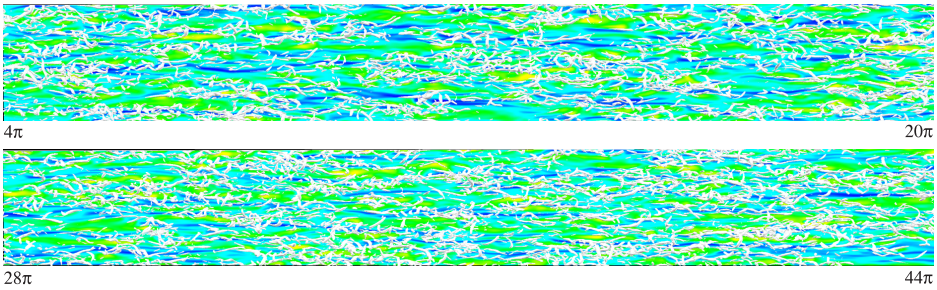

Fig. 14 Contour of streamwise velocity on a $x-z$ plane ($y^+ \approx 10$) with iso-surface of $Q = 1.0$ for case1.

In downstream, Nusselt number in the cooling region is higher than that in the heating region. This is an expected result by considering physical properties in the high and low temperature side. According to physical properties of supercritical CO_2, the Prantdl number increases dramatically if temperature is close to the pseudo-critical point, which leads to high Nusselt number in the cooling region. Figure 11 shows the turbulent heat flux $\overline{v'T'}$ at $x = 15.9\pi$ (in the heating region) and $-\overline{v'T'}$ at $x = 41.4\pi$ (in the cooling region) for case1. Compared with the heating region, the enhanced turbulence in the cooling region leads to higher turbulent heat flux. The difference of the peak magnitude of the heat flux is about 30%. The location of the peak is shifted into large y^+ in the cooling region. The high local Re_τ in the cooling region leads to the high turbulent heat flux. This enhancement of heat flux results in high Nusselt number in the cooling region as shown in Fig. 10.

Figure 12 shows distribution of kinematic viscosity and thermal conductivity on a x-z plane at $y^+ \approx 5$ for case1. Here, darker regions represents lower kinematic viscosity or thermal conductivity. High thermal conductivity and low kinematic viscosity are observed in the

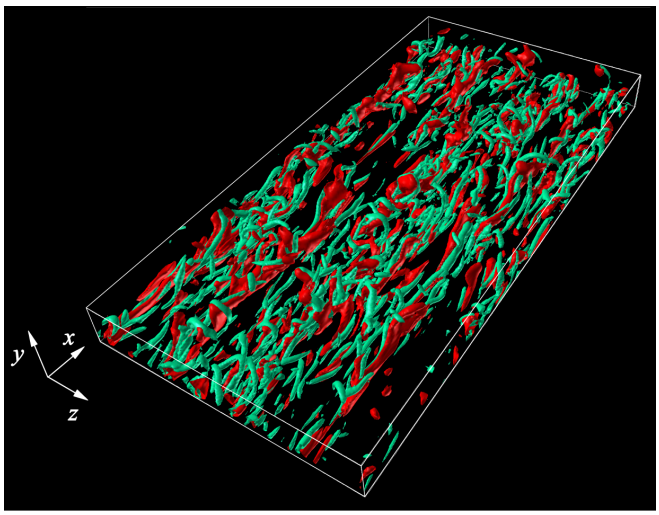

Fig. 15 Iso-surface of $Q = 1.0$ (green) with iso-surface of $v'T' = 1.0 \times 10^{-4}$ (red), $12\pi < x < 16\pi$ in case1.

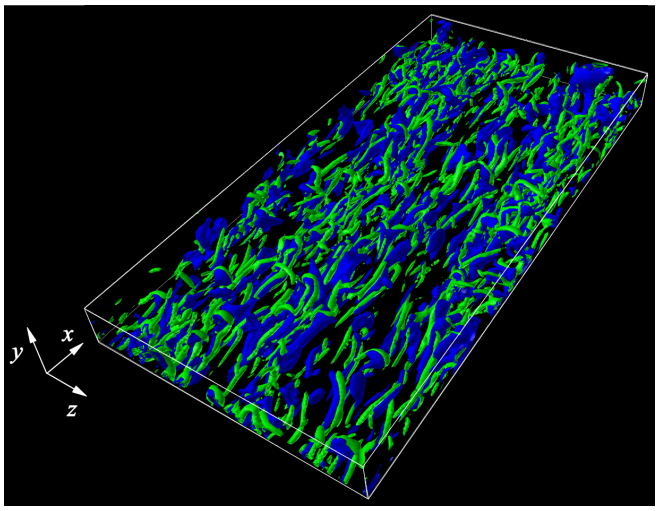

Fig. 16 Iso-surface of $Q = 1.0$ (green) with iso-surface of $v'T' = -1.0 \times 10^{-4}$ (blue), $36\pi < x < 40\pi$ in case1.

cooling region. Both kinematic viscosity and thermal conductivity show streaky distribution in the heating and cooling region. The size of these streaky structures in the cooling region decreases compared with that in the heating region as shown in Fig. 6, which indicates that turbulence is enhanced in the cooling region as shown in Fig. 5. The enhanced turbulence and high thermal conductivity in the cooling region result in high Nusselt number.

As is expected from turbulence statistics in above, turbulence structures near the wall are modified by temperature dependence of transport and thermal properties of the supercritical CO_2. Figure 13 shows distribution of temperature on a x-z plane ($y^+ \approx 10$) with iso-surfaces of the second invariant of velocity gradient tensor ($Q = 1.0$) in case1. The second invariant is defined by

$$Q = \frac{1}{2}(-S_{ij}S_{ij} + W_{ij}W_{ij}), \tag{10}$$

where S_{ij} and W_{ij} denotes symmetric and antisymmetric part of the velocity gradient tensor ($A_{ij} = \partial u_i/\partial x_j$). The positive Q regions can represent fine scale vortical structures[7),(11),(12)]. Near the wall, the positive Q regions in the normalization based on the outer quantities represent near-wall eddy structures such as streamwise eddies and hairpin-vortices. These struc-

tures are one kind of the coherent fine scale eddy as reported by Tanahashi et al.[7]. Temperature is denoted by colors (high temperature is denoted by red). In Fig. 14, streamwise velocity fluctuation of case1 is shown in a same way. The number of the fine scale eddy in the heating region is obviously less than that in the cooling region. In the heating region, the coherent fine scale eddies tend to exist in high temperature and low speed streaks. From the characteristics of supercritical CO_2, since high temperature regions possesses high kinematic viscosity, fine scale eddies might disappear with the heating of the fluid in the downstream. On the other hand, in the cooling region, the coherent fine scale eddies tend to exist in low temperature and high speed streaks. In the downstream, lots of hairpin-like eddies can be observed. Contrary to the heating region, low temperature regions possesses low kinematic viscosity. Therefore, fine scale eddies might be created continuously in the downstream.

These relations between fine scale eddy and temperature have great importance in the heat transfer near the wall. In the heating region, high temperature corresponds to low Prandtl number. In the cooling region, high Prandtl number due to low temperature enhances temperature fluctuation in small scales, which results in effective mixing by the fine scale eddy. These combined effects of turbulence structure and turbulent mixing have significant contributions to low Nusselt number in the heating region and high Nusselt number in the cooling region in Fig. 10.

The modifications of turbulence structure and mixing mechanism also affect the turbulent heat flux near the wall. In Figs. 15 and 16, instantaneous turbulent heat flux ($v'T'$) is shown in the heating and cooling regions with isosurfaces of Q for case1. The threshold of the turbulent heat flux is selected to $v'T' = \pm 1.0 \times 10^{-4}$ which is about three times larger (or smaller) than that of mean values shown in Fig. 11. In the heating region, high heat flux regions exist along the fine scale eddies and are localized near the wall. However, in the cooling region, high heat flux region are extended into the channel center. The high heat flux region far from the wall possesses hairpin-like feature, and hairpin-like fine scale eddies, which are enhanced by local high Reynolds number effect, also exist in these regions. These results suggest that the modified turbulence structure causes high turbulent heat flux in the cooling region.

7. CONCLUSIONS

Direct numerical simulation of supercritical CO_2 turbulent channel flow is preformed by considering temperature dependence of thermal and transport properties. In DNS, full compressible Navier-Stokes equations are treated with Peng-Robinson state equation. From DNS results, difference between the heating and cooling process of supercritical CO_2 is discussed in the temperature range higher than the pseudo-critical point.

Mean velocity in the cooling region becomes high compared with that in the heating region, whereas the Van Direst velocities at two regions agree very well. These results suggest that mean velocity is affected by density variation, but not by acoustic effects or intrinsic compressibility effects. Compressibility effects related with pressure fluctuation and dilatation of velocity fluctuation can be ignored in the transport of turbulent kinetic energy, whereas the effect of density fluctuation on turbulent kinetic energy cannot be ignored. The production and viscous dissipation terms tend to increase near the pseudo-critical temperature. The terms related to density fluctuations, which partially offset the turbulent kinetic energy, become significant near the pseudo-critical temperature.

The mean width between high- and low-speed streaks near the wall decreases in the cooling region and number of those increases. The low speed and low temperature regions near the wall enhances fine scale motion of the fluid in the cooling side, which results in the increase of the coherent fine scale eddy. Since low temperature regions in the cooling side correspond to high thermal conductivity regions, temperature mixing by the fine scale eddy is enhanced. The turbulent heat flux is also intensified by the modification of the turbulence structures due to the local high Reynolds number effects. These combined effects result in high Nusselt number in the cooling condition of the supercritical CO_2.

REFERENCES

(1) Oka, Y., and Koshizuka, S., 2000. Design concept of once-through cycle super-critical pressure light water cooled reactors, In proceedings of the first international symposium on supercritical water-cooled reactor design (SCR-2000), Paper No. 101, The University of Tokyo, Tokyo, Japan.

(2) Hashimoto, K., Hirasawa, K., Tanahashi, M. and Miyauchi, T., 2005. DNS of turbulent heat transfer of cabon dioxide in supercritical condition, In proceedings of 4th international conference on computational heat and mass transfer, Pris-Cachan, France.

(3) Bae, J.H. and Yoo, J.Y., 2005. Direct numerical simulation of turbulent supercritical flows with heat transfer, Physics of Fluids, Vol. 17, No.10, Art. No. 105104.

(4) Peng, D.Y. and Robinson, D.B., 1976. New 2-constant equation of state. Industrial & Engineering Chemisty Fundamentals, Vol. 15, No. 1, p59-64.

(5) Span, R. and Wagner, W.J., 1996. A new equation of state for carbon dioxide covering temperature to 110K at pressure up to 800MPa, Journal of Physical Chemistry Reference Data, Vol. 25, No. 6, p1509-1596.

(6) Jiang, G.S. and Shu, C. W., 1996. Efficient implementation of weighted ENO schemes, Journal of Computational Physics, Vol. 126, p202-228.

(7) Tanahashi, M., Kang, S.J., Miyamoto, T., Shiokawa, S. and Miyauchi, T., 2004. Scaling law of fine scale eddies in turbulent channel flows up to Re_τ = 800, International Journal of Heat and Fluid Flow, Vol. 25, p331-340.

(8) Pirozzoli, S. and Grasso F., 2004. Direct numerical simulation and analysis of a spatially evolving supersonic turbulent boundary layer at M=2.25, Physics of Fluids, Vol. 16, No. 3, p530.

(9) Kim, J., Moin, P. and Moser, R.D., 1987. Turbulence statistics in fully developed channel flow at low Reynolds number, Journal of Fluid Mechanics, Vol. 177, p133-166.

(10) Moser, R.D., Kim, J. and Mansour, N.N., 1999. Direct numerical simulation of turbulent channel flow up to Re_τ = 590, Physics of Fluids, Vol. 11, No.4, p943-945.

(11) Tanahashi, M., Miyauchi, T. and Ikeda, J., 1999. Simulation and Identification of Organized Structures in Flows, Kluwer Academic Publishers, p131-140.

(12) Tanahashi, M., Iwase, S. and Miyauchi, T., 2001. Appearance and alignment with strain-rate of coherent fine scale eddies in turbulent mixing layer, Jounal of Tubulence, 2, p6.